

# Computational Synthesis of MoS<sub>2</sub> Layers by Reactive Molecular Dynamics Simulations: Initial Sulfidation of MoO<sub>3</sub> Surfaces

Sungwook Hong\*,†,‡ Aravind Krishnamoorthy, † Pankaj Rajak, † Subodh Tiwari, † Masaaki Misawa, ‡ Fuyuki Shimojo, † Rajiv K. Kalia, † Aiichiro Nakano, † and Priya Vashishta †

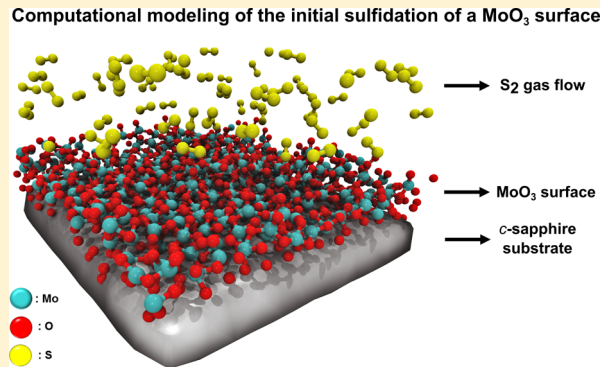
†Collaboratory for Advanced Computing and Simulations, Department of Physics & Astronomy, Department of Computer Science, Department of Chemical Engineering & Materials Science, and Department of Biological Sciences, University of Southern California, Los Angeles, California 90089-0242, United States

‡Department of Physics, Kumamoto University, Kumamoto 860-8555, Japan

## Supporting Information

**ABSTRACT:** Transition metal dichalcogenides (TMDC) like MoS<sub>2</sub> are promising candidates for next-generation electric and optoelectronic devices. These TMDC monolayers are typically synthesized by chemical vapor deposition (CVD). However, despite significant amount of empirical work on this CVD growth of monolayered crystals, neither experiment nor theory has been able to decipher mechanisms of selection rules for different growth scenarios, or make predictions of optimized environmental parameters and growth factors. Here, we present an atomic-scale mechanistic analysis of the initial sulfidation process on MoO<sub>3</sub> surfaces using first-principles-informed ReaxFF reactive molecular dynamics (RMD) simulations. We identify a three-step reaction process associated with synthesis of the MoS<sub>2</sub> samples from MoO<sub>3</sub> and S<sub>2</sub> precursors: O<sub>2</sub> evolution and self-reduction of the MoO<sub>3</sub> surface; SO/SO<sub>2</sub> formation and S<sub>2</sub>-assisted reduction; and sulfidation of the reduced surface and Mo–S bond formation. These atomic processes occurring during early stage MoS<sub>2</sub> synthesis, which are consistent with experimental observations and existing theoretical literature, provide valuable input for guided rational synthesis of MoS<sub>2</sub> and other TMDC crystals by the CVD process.

**KEYWORDS:** ReaxFF, molecular dynamics simulations, MoO<sub>3</sub> surface, sulfidation, MoS<sub>2</sub>, synthesis



Two-dimensional and layered materials have unique electric and optoelectronic characteristics, distinct from their bulk phases due to the existence of relatively weak interlayer interactions and two-dimensional quantum confinement.<sup>1–3</sup> Graphene was the first to be considered a real two-dimensional material,<sup>4</sup> and it has been extensively studied for nanoscale applications.<sup>4,5</sup> Two-dimensional semiconducting crystals like MoS<sub>2</sub> monolayer are promising candidates for next-generation electronic devices (e.g., ultrathin channel materials) primarily due to (a) the high abundance of molybdenite and the associated low cost, (b) greater carrier mobility than conventional Si-based devices, and (c) nonzero bandgaps, unlike graphene.<sup>6–8</sup> In addition, MoS<sub>2</sub> monolayer can be applied to flexible substrates because of its exceptional mechanical properties<sup>9–12</sup> and can provide active edge sites for the hydrogen evolution reaction.<sup>13</sup> MoS<sub>2</sub> samples for bench-scale devices and experiments are typically synthesized via mechanical exfoliation or chemical vapor deposition (CVD).<sup>14–16</sup> Of these two methods, CVD is the only method that can be scaled up for mass production of monolayered crystals required into consumer applications. While several previous studies have demonstrated the growth of MoS<sub>2</sub> layers from different precursors and have provided qualitative

information about reaction pathways leading to crystal growth,<sup>17–23</sup> deciphering selection rules for different growth scenarios to make predictions of optimized environmental parameters and growth factors has remained unclear. This is primarily due to a lack of understanding of mechanistic processes by which the CVD growth of MoS<sub>2</sub> monolayer is achieved. Computational modeling, particularly reactive molecular dynamics (RMD) simulations, can provide useful insights into interfaces<sup>24</sup> and surface–gas interactions<sup>25</sup> on model systems down to atomic length scales. In this work, we perform RMD simulations for computational synthesis of MoS<sub>2</sub> structures using MoO<sub>3</sub> surfaces and gaseous S<sub>2</sub>. Our goal is to identify the atomic-level mechanism for the growth of MoS<sub>2</sub> phases by the sulfidation of MoO<sub>3</sub> crystals. The subsequent sections describe the computational methodology for RMD simulations followed by a discussion of the observed mechanism for the reaction between MoO<sub>3</sub> and S<sub>2</sub> to form MoS<sub>2</sub>.

**Received:** April 24, 2017

**Revised:** June 29, 2017

**Published:** July 3, 2017



Empirical reactive methods such as the COMB<sup>26,27</sup> and ReaxFF<sup>28</sup> potentials allow for large-scale RMD simulations with a well-documented variable-charge scheme.<sup>29</sup> In this study, ReaxFF reactive force field parameters for Mo/O and Mo/S interactions were extracted from Chenoweth et al.<sup>30</sup> and Ostadhosseini et al.,<sup>31</sup> respectively, and then reoptimized to more accurately describe reaction events between the MoO<sub>3</sub> surface and S<sub>2</sub> molecules. In addition, ReaxFF reactive force field parameters for S/O interactions, successfully applied to a previous study,<sup>32</sup> were taken to capture CVD processes; the Supporting Information includes quantum mechanical (QM) data used for a ReaxFF force field training set and results of the force field reoptimization. Detailed information on ReaxFF and its applications is available in review papers.<sup>33,34</sup> ReaxFF force field parameters were then coupled with RMD simulations. Small integration time steps of 0.25–0.30 fs were used with the NVT ensemble to properly describe chemical reactions. To control system temperatures, the Nose–Hoover thermostat<sup>35,36</sup> with a temperature damping constant of 25.0 fs was applied to the whole system including gas and surface models. We simulated a MoO<sub>3</sub> layer supported on an Al<sub>2</sub>O<sub>3</sub> substrate, exposed to S<sub>2</sub> atmosphere, following a recent experimental setup (Figure 1a).<sup>21</sup> All simulations were done on a simulation

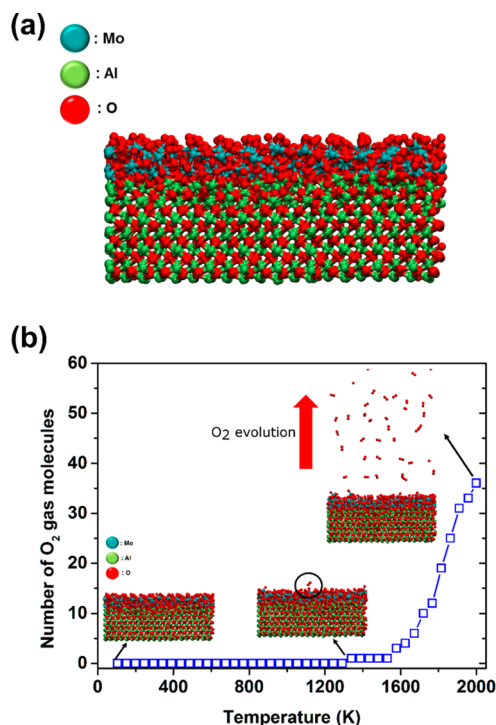


**Figure 1.** (a) Initial configuration of the MoO<sub>3</sub>/Al<sub>2</sub>O<sub>3</sub> surface. The surface was annealed at 500 K for 125 ps and cooled down to 100 K for 25 ps. (b) Number of O<sub>2</sub> gas molecules evolved from the MoO<sub>3</sub> surface as a function of instantaneous temperature, and corresponding RMD snapshots at 0, 1300, and 2000 K. The black circle in the snapshot at 1300 K represents the onset of O<sub>2</sub> evolution.

cell of lateral dimensions (47.09 Å × 45.57 Å) containing one monolayer of MoO<sub>3</sub> (~6 Å thick) supported on an Al<sub>2</sub>O<sub>3</sub> (0001) surface (~15 Å thick); the Al<sub>2</sub>O<sub>3</sub> surface serves as a substrate, while MoO<sub>3</sub> surface provides Mo sources on the substrate for the growth of MoS<sub>2</sub> structures. This combined surface structure, consisting of the α-MoO<sub>3</sub>(001) surface (1152 atoms) supported by the α-Al<sub>2</sub>O<sub>3</sub>(0001) surface (3375 atoms)

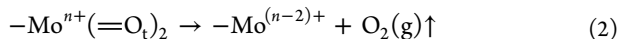
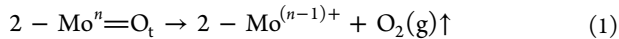
was relaxed using a conjugate gradient method, followed by thermal equilibration at 500 K for 125 ps, and then cooled down to 100 K for 25 ps. This simulation schedule leads to a model of a MoO<sub>3</sub> predeposited on Al<sub>2</sub>O<sub>3</sub>, consistent with experimental studies.<sup>21,37</sup> For CVD synthesis of atomically thin MoS<sub>2</sub> layers, both MoO<sub>3</sub> and S powders are generally employed as initial reactants. However, the experimental studies in refs 21 and 37 indicated that wafer-scale MoS<sub>2</sub> layers with great uniformity can be effectively synthesized by using a predeposited MoO<sub>3</sub> surface, instead of vaporized MoO<sub>3</sub> powder, as a starting material. Thus, we chose to use the predeposited MoO<sub>3</sub> surface on the Al<sub>2</sub>O<sub>3</sub> surface for RMD simulations. Although our simulation model is dissimilar to the one from experimental methods typically using MoO<sub>3</sub> and sulfur powders,<sup>38,39</sup> our study still provides key reaction events for the sulfidation of MoO<sub>3</sub> that eventually enables us to understand the conventional CVD process of MoS<sub>2</sub> layers. Furthermore, as discussed above, our simulation model is consistent with the experimental setup that used the MoO<sub>3</sub> predeposited on Al<sub>2</sub>O<sub>3</sub> substrate, thus providing a better understanding of reaction mechanisms for the sulfidation of the MoO<sub>3</sub> surface using S<sub>2</sub> gas molecules. For CVD simulations, we placed the surface model along with gaseous S<sub>2</sub> in vacuum layers of 100 Å. In doing so, CVD processes can be reproduced by our RMD simulations using chemical reactions of the MoO<sub>3</sub> surface and S<sub>2</sub> gas molecules. In light of relatively high temperatures during our ReaxFF-RMD simulations (up to 2300 K), compared to experimental CVD conditions (~1200 K),<sup>40,41</sup> a one-body spring force was added to each atom in the α-Al<sub>2</sub>O<sub>3</sub>(0001) surface to prevent interdiffusion of the Al<sub>2</sub>O<sub>3</sub> and MoO<sub>3</sub>. This ensures that the α-Al<sub>2</sub>O<sub>3</sub>(0001) surface behaves as a nonreactive surface for our RMD simulations. In addition, a periodic boundary condition was used in the *x*- and *y*-directions, while a wall boundary condition was applied to the *z*-direction to prevent the diffusion of gas-phase atoms across the boundary and potentially reacting with the bottom of the α-Al<sub>2</sub>O<sub>3</sub> surface.

Our RMD simulations identify a three-step reaction pathway for the synthesis of MoS<sub>2</sub> crystals by the sulfidation (by S<sub>2</sub> gas) of MoO<sub>3</sub> monolayers: 1. O<sub>2</sub> evolution and self-reduction of the MoO<sub>3</sub> surface; 2. SO/SO<sub>2</sub> formation and S<sub>2</sub>-assisted reduction; 3. Sulfidation of the reduced surface and Mo–S bond formation. This section reports the three reaction processes stepwise.

#### O<sub>2</sub> Evolution and Self-Reduction of the MoO<sub>3</sub> Surface.

To elucidate the surface chemistry of MoO<sub>3</sub>(001) at high temperatures, the MoO<sub>3</sub>/Al<sub>2</sub>O<sub>3</sub> surface (see Figure 1a) was heated from 100 to 2000 K at a heating rate of 0.002 K/fs. Figure 1b shows the number of O<sub>2</sub> gas molecules evolved from the MoO<sub>3</sub> surface as a function of the instantaneous temperature of the system, described by the ReaxFF-RMD simulations. O<sub>2</sub> evolution begins at approximately 1300 K, which lies above the reported melting point and below the sublimation point of the MoO<sub>3</sub> crystal,<sup>42</sup> suggesting that O<sub>2</sub> evolution occurs from a disordered, noncrystalline MoO<sub>3</sub> structure. Our RMD simulations show that O<sub>2</sub> molecules are predominantly generated due to the cleavage of the terminal Mo=O<sub>t</sub> double bonds or the weaker, asymmetric bridging Mo–O–Mo bonds in-plane. Basically, our ReaxFF description has shown its ability to reasonably describe bulk properties and thermal stabilities of α-phase MoO<sub>3</sub> crystal structure, consistent with experimental and density functional theory (DFT) literature (see Supporting Information for details of ReaxFF

reactive force field validation). In addition, based on previous experimental observations,<sup>43</sup> the O-termination site in crystalline MoO<sub>3</sub> is known to be the most reactive entity, thus preferably reacting with each other and leading to O<sub>2</sub> evolution. Namely, the mechanisms for O<sub>2</sub> evolution and MoO<sub>3</sub> reduction by our RMD simulations are in excellent agreement with experimental observations in ref 43 as follows:



To evaluate the unit processes involved in O<sub>2</sub> evolution from the MoO<sub>3</sub> surface in more detail and to quantify the effect of structural disorder on O<sub>2</sub> evolution, we performed ReaxFF-nudged elastic band (ReaxFF-NEB) calculations to evaluate activation barriers. Specifically, we compared reaction paths calculated for identical O<sub>2</sub> evolution reactions on MoO<sub>3</sub> surfaces at low and high temperatures. Low-temperature surface structures correspond to the 0 K ground state structure of the MoO<sub>3</sub>(001) surface, while high-temperature structures are constructed from snapshots of the RMD simulations at an instantaneous temperature of 2000 K. Figure 2 demonstrates

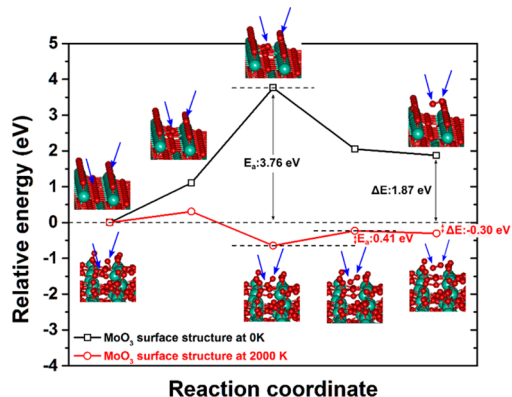


**Figure 2.** ReaxFF-NEB calculations of reaction paths for the O<sub>2</sub> evolution at the MoO<sub>3</sub> surface structure 0 K (black hollow square) and 2000 K (red hollow circle). Blue arrows represent O atoms participating in the O<sub>2</sub> evolution; one originates from the O-termination site and the other one from the Mo–O–Mo bridge. Note that the distorted MoO<sub>3</sub> structure (2000 K) lowers the largest reaction barrier to 0.41 eV and changes the reaction to exothermic ( $-0.30$  eV), making the O<sub>2</sub> evolution favorable thermodynamically and kinetically (cyan balls and sticks, Mo atoms; red balls and sticks, O atoms).

that O<sub>2</sub> evolution from the distorted high-temperature surface is moderately exothermic ( $\Delta E = -0.30$  eV) and has an activation barrier of 0.41 eV, in contrast to the crystalline ground-state surface, which shows a high endothermicity and a high activation barrier ( $\Delta E = 1.87$  eV,  $E_a = 3.76$  eV) that renders O<sub>2</sub> evolution kinetically and energetically unfavorable at low temperatures. These results suggest that high-temperature-induced structural distortion is necessary for O<sub>2</sub> evolution, which leads to the generation of unsaturated Mo sites on the MoO<sub>3</sub> surface for subsequent sulfidation.

To investigate the kinetics of the thermal reduction process on MoO<sub>3</sub> surfaces, we held the MoO<sub>3</sub>/Al<sub>2</sub>O<sub>3</sub> surface described previously at a high temperature of 2000 K for 775 ps, and followed the O<sub>2</sub> evolution process as a function of time. As shown in Figure 3a, the number of O<sub>2</sub> gas molecules displays

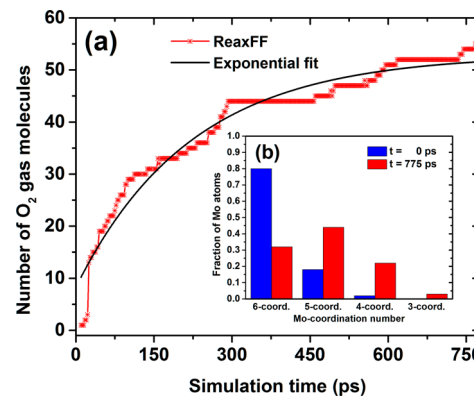


**Figure 3.** ReaxFF-RMD simulations of O<sub>2</sub> evolution from a MoO<sub>3</sub> surface held at 2000 K. (a) Number of O<sub>2</sub> gas molecules evolved as a function of time at 2000 K. (b) Histogram of coordination number of Mo atoms in the MoO<sub>3</sub> surface in the low-temperature, stoichiometric crystal (blue) compared with the reduced surface after 775 ps of reduction at 2000 K. At 100 K (0 ps), most Mo-coordination consisted of 6-coordination (a small portion of 5- and 4-coordination was also observed because the initial MoO<sub>3</sub>/Al<sub>2</sub>O<sub>3</sub> surface was thermally equilibrated at 500 K and thus the atoms' positions were rearranged). At 2000 K (775 ps), the 6-coordination was reduced to 5-, 4-, and 3-coordination, indicating that the number of unsaturated Mo atoms increased.

monotonic exponential kinetics, leading to a partially reduced MoO<sub>2.6</sub> surface at 775 ps. Figure 3b shows the histogram for coordination number for Mo atoms in the MoO<sub>3</sub> surface at  $t = 0$  and  $t = 775$  ps. O<sub>2</sub> evolution during the high-temperature annealing process causes the 6-fold coordinated Mo atoms at low temperature to become undersaturated 5-fold, 4-fold, and 3-fold coordinated Mo atoms (i.e., self-reduction), which act as reaction sites for subsequent sulfidation reactions.

**SO/SO<sub>2</sub> Formation and S<sub>2</sub>-Assisted Reduction.** To investigate whether the undersaturated Mo atoms activate toward subsequent sulfidation, we performed first-principles QM calculations based on DFT. Section 2.3 in the *Supporting Information* shows DFT-based nudged elastic band (DFT-NEB) calculations of S<sub>2</sub> adsorption on a MoO<sub>3</sub>(010) with an O-vacancy. The DFT-NEB calculations were also used to validate the ReaxFF force field. The ReaxFF-NEB results on reaction barrier (0.22 eV) and energy ( $-1.11$  eV) for the S<sub>2</sub> adsorption on the MoO<sub>3</sub> (010) with an O-vacancy quantitatively agree with our DFT-NEB calculations, thus validating the ReaxFF force field for this key reaction. The relatively low barrier and high exothermicity suggest that the reduced MoO<sub>x</sub> surface is necessary for making sulfidation reactions preferable.

Based on this observation, the reduced MoO<sub>2.6</sub>/Al<sub>2</sub>O<sub>3</sub> surface from the previous section was then placed in contact with an atmosphere of 400 S<sub>2</sub> gas molecules in the simulation cell (corresponding to a density of S<sub>2</sub> gas: 0.23 g/cm<sup>3</sup>) to perform ReaxFF-RMD simulations of the sulfidation process. Figure 4a,b shows the initial and final snapshots of the ReaxFF-RMD simulations at 2300 K, respectively. After 1.2 ns, it is worth noting that S<sub>2</sub> gas molecules reacted with the MoO<sub>2.6</sub> surface, leading to the formation of SO and SO<sub>2</sub> gas products (inset in Figure 4b). Based on trajectories of the ReaxFF-RMD simulations, the primary reaction mechanisms for SO and SO<sub>2</sub> formation can be summarized as follows:

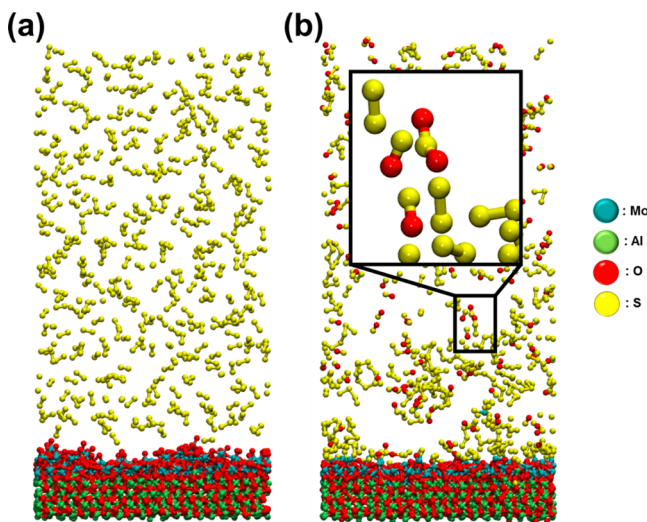
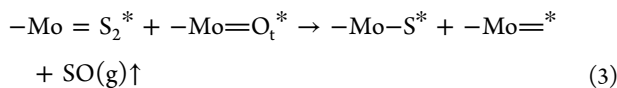


**Figure 4.** Snapshots of sulfidation at the  $\text{MoO}_{2.6}/\text{Al}_2\text{O}_3$  surface described by the ReaxFF-RMD simulations (a) at 0 ns and (b) at 1.2 ns. Note that 97% of gas products consists of  $\text{SO}$  molecules (3% for  $\text{SO}_2$  molecules).



where an asterisk represents a surface species.  $\text{S}_2$  molecules were found to participate both in the further reduction of the  $\text{MoO}_{2.6}$  structure as well as the sulfidation of the reduced surface, thus validating mechanisms hypothesized in a previous experimental study.<sup>44</sup> In addition, the reaction mechanisms described by our RMD simulations were qualitatively consistent with a previous study<sup>22</sup> reporting that  $\text{MoO}_3$  reactants are reduced by sulfur gas to form oxy sulfide species ( $\text{MoO}_{x,y}$ ), resulting in the formation of  $\text{SO}_x$  products. Consequently, the  $\text{MoO}_{2.6}$  surface transformed to a  $\text{MoO}_{1.99}\text{S}_{0.24}$  surface structure (Table 1). To support the robustness of the ReaxFF description for describing the surface reactions above, we constructed ground-state structures containing  $\text{S}_2/\text{MoO}_3$  surface interactions:  $\text{S}_2$  dissociation on the  $\text{MoO}_3$  surface and  $\text{SO}_2$  desorption from the  $\text{MoO}_3$  surface. Then, DFT- and ReaxFF-NEB calculations were conducted to investigate reaction energies and barriers (see Supporting Information for details of DFT-NEB calculations). As shown in Figure 5a,b, the reaction barriers and energies of the above cases, as proposed

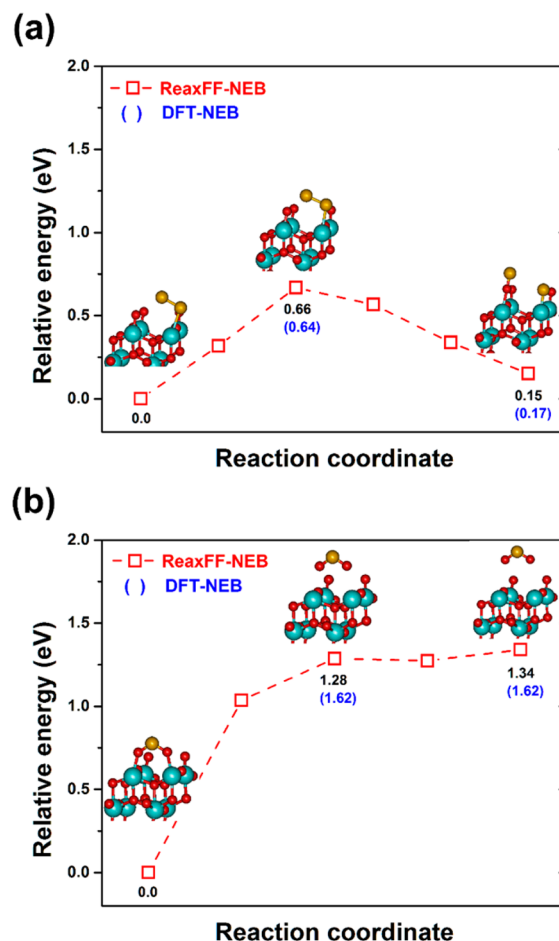


**Figure 5.** ReaxFF-NEB calculations of reaction paths for (a)  $\text{S}_2$  dissociation from the O-vacancy site on the  $\text{MoO}_3$  surface and (b)  $\text{SO}_2$  desorption from the O-vacancy site on the  $\text{MoO}_3$  surface. The initial  $\text{MoO}_3$  surface structure was taken from the ground state structure. Reaction barriers and energies from the DFT-NEB calculations (blue parentheses) indicate that the ReaxFF can correctly capture reaction events associated with  $\text{S}_2/\text{MoO}_3$  interactions (cyan, Mo atoms; red, O atoms; yellow, S atoms).

by the ReaxFF-NEB calculations, were quantitatively consistent with the DFT-NEB calculations, thus validating the ability of the ReaxFF description to properly capture reaction events between  $\text{S}_2$  gas and the  $\text{MoO}_3$  surface. The ReaxFF-NEB results indicate that  $\text{S}_2$  dissociation on the  $\text{MoO}_3$  surface is somewhat endothermic (reaction energy of 0.15 eV) with a mild barrier

**Table 1.** Surface Structures of  $\text{MoO}_{x,y}$  Obtained by the Stepwise ReaxFF-RMD Simulations<sup>a</sup>

simulation step	temperature (K)	accumulated time (ns)	number of atoms of each species on the reacting surface			surface composition
			Mo	O	S	
initial	0	0.000	288	864	0	$\text{MoO}_3$
annealing	2000	0.775	288	748	0	$\text{MoO}_{2.60}$
sulfidation	2300	1.975	286	571	70	$\text{MoO}_{1.99}\text{S}_{0.24}$
sulfidation	2300	3.175	286	539	99	$\text{MoO}_{1.88}\text{S}_{0.35}$
sulfidation	2300	7.975	263	447	147	$\text{MoO}_{1.70}\text{S}_{0.56}$
cooling	300	8.125	263	447	147	$\text{MoO}_{1.70}\text{S}_{0.56}$

<sup>a</sup>An annealing process was conducted for the first 0.775 ns, followed by a sulfidation process for a further 7.200 ns. Subsequently, the surface structure was cooled down to 300 K for 0.150 ns. During the sulfidation process, all gas products were removed, and intact  $\text{S}_2$  gas molecules were added every 1.2 ns. Note that the initial  $\text{MoO}_3$  surface structure converted to a  $\text{MoO}_{1.70}\text{S}_{0.56}$  surface structure at the accumulated time of 8.125 ns.

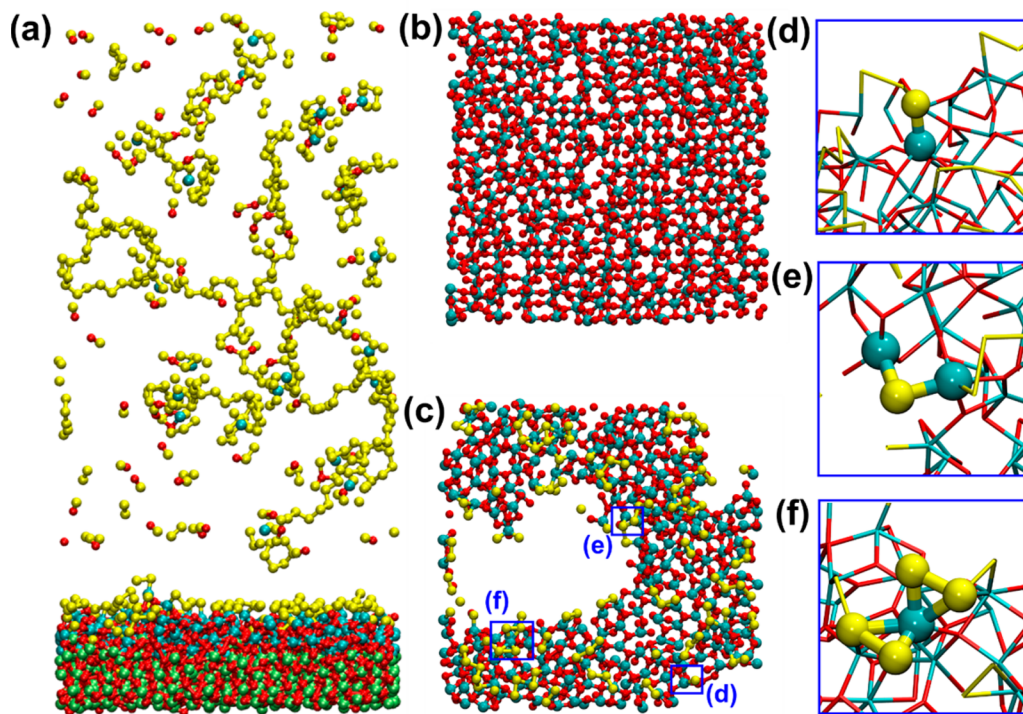


**Figure 6.** (a) Snapshot of the RMD simulation cell at 8.125 ns. (b,c) Top views of the MoO<sub>3</sub> (0 ns) and MoO<sub>1.70</sub>S<sub>0.56</sub> surface (8.125 ns) structures, respectively; Al and O atoms in the Al<sub>2</sub>O<sub>3</sub> layer are hidden for clarity. Significant voids were observed on the MoO<sub>1.70</sub>S<sub>0.56</sub> surface due to Mo atoms' redistribution during the reduction and sulfidation processes. (d–f) Close-ups of Mo–S termination, Mo–S–Mo bridge, and Mo(S<sub>2</sub>)<sub>2</sub> edge structures, respectively, as highlighted in (c). Note that three structures describe a small portion of MoS<sub>2</sub> structures, which can be further grown to form MoS<sub>2</sub>-like crystals (cyan balls and sticks, Mo; lime balls and sticks, Al; red balls and sticks, O; yellow balls and sticks, S).

(0.66 eV), and that the SO<sub>2</sub> desorption from the MoO<sub>3</sub> surface is a much more unfavorable reaction, as the total energy increased to 1.34 eV. As such, one can expect that surface reactions associated with SO<sub>2</sub> formation will be energetically unfavorable compared with SO formation. These analyses can aid in explaining the observation of a relatively large number of SO gas products (97% of gas products), compared to that of the SO<sub>2</sub> gas products (3% of gas products) during the ReaxFF-RMD simulations at 2300 K. Therefore, we suggest that further reduction and sulfidation of the MoO<sub>2.6</sub> surface can be achieved by two reaction processes at high temperatures: primarily SO formation, followed by SO<sub>2</sub> formation.

**Sulfidation of the Reduced Surface and Extensive Mo–S Bond Formation.** To further observe Mo–S bonds formation, we extended our ReaxFF-RMD simulations for the sulfidation at the partially reduced and partially sulfurized MoO<sub>1.99</sub>S<sub>0.24</sub> surface from the previous section for a further 6.0 ns, after which the final surface structure was cooled down to 100 K for additional 0.15 ns. In order to simulate the flow of the gas phase over the reacting surface in CVD growth conditions, all gas molecules in the simulation cell were purged every 1.2 ns and replaced with pure S<sub>2</sub> molecules. Figure 6a shows a final snapshot of the surface structure from the ReaxFF-RMD simulations. As shown in Table 1, the final structure at an accumulated reaction time of 8.125 ns corresponds to a MoO<sub>1.70</sub>S<sub>0.56</sub> surface, indicating that further O atoms in the MoO<sub>x</sub>S<sub>y</sub> surface were substituted by S atoms and additional S<sub>2</sub> molecules chemisorbed on the MoO<sub>x</sub>S<sub>y</sub> surface. It is interesting to note that, during the ReaxFF-RMD simulations of the sulfidation process, significant voids on the Al<sub>2</sub>O<sub>3</sub> substrate were generated as the initial MoO<sub>3</sub> surface

structure converted to the MoO<sub>1.70</sub>S<sub>0.56</sub> surface structure, resulting in the Mo atoms' migration and reorganization on the Al<sub>2</sub>O<sub>3</sub> substrate (see Figure 6b,c). These results are consistent with the early stage of the sulfidation process at the MoO<sub>3</sub> predeposited sapphire substrate by Taheri et al.<sup>37</sup> Their experimental study reported that the growth of MoS<sub>2</sub> monolayer involved not only S substitutions on the MoO<sub>3</sub> surface but also Mo atoms' redistribution, and thus, voids were observed when forming discrete MoS<sub>2</sub> triangles. In addition, Mo/S configurations on the final MoO<sub>1.70</sub>S<sub>0.56</sub> surface structure qualitatively matched with a portion of monolayered MoS<sub>2</sub> crystal structure; the Mo/S structures from the ReaxFF-RMD simulations exhibit a proportion of S-termination, Mo–S–Mo bridge, and MoS<sub>2</sub> edge structures, as shown in Figure 6d–f, respectively. Based on our observations, it is expected that when exposing to more S<sub>2</sub> gas flow, surface structures like stoichiometric MoS<sub>2</sub> crystals can be synthesized. While further growth and follow-up crystallization of MoS<sub>2</sub> monolayers will be studied in the future, the present ReaxFF-RMD simulations confirm that the initial sulfidation process of the MoO<sub>3</sub> surface is achieved by three reaction steps.

In summary, we investigated the computational synthesis of MoS<sub>2</sub> layers from deposited MoO<sub>3</sub> and gaseous S<sub>2</sub> precursors using ReaxFF-RMD simulations with reoptimized force field parameters for Mo/O/S. The ReaxFF-RMD simulations demonstrated that a portion of the MoS<sub>2</sub> species can be synthesized via a three-step reaction mechanism: 1. O<sub>2</sub> evolution and self-reduction of the MoO<sub>3</sub> surface, 2. SO/SO<sub>2</sub> formation and S<sub>2</sub>-assisted reduction, and 3. Sulfidation of the reduced surface and Mo–S bond formation. The atomic resolution of the RMD simulations allows us to elucidate

important details about the synthesis process, like the requirement of a disordered surface structure, and the dual role of S<sub>2</sub> molecules as reducing and sulfidizing agents. In that sense, our approach opens a promising direction to explore complex reaction processes for synthesis of MoS<sub>2</sub> monolayers, and other two-dimensional materials.

## ■ ASSOCIATED CONTENT

### S Supporting Information

The Supporting Information is available free of charge on the ACS Publications website at DOI: [10.1021/acs.nanolett.7b01727](https://doi.org/10.1021/acs.nanolett.7b01727).

ReaxFF reactive force field reoptimization and validation for Mo/O/S interactions ([PDF](#))

## ■ AUTHOR INFORMATION

### Corresponding Author

\*E-mail: [sungwooh@usc.edu](mailto:sungwooh@usc.edu).

### ORCID

Sungwook Hong: [0000-0003-3569-7701](https://orcid.org/0000-0003-3569-7701)

Aravind Krishnamoorthy: [0000-0001-6778-2471](https://orcid.org/0000-0001-6778-2471)

### Author Contributions

S.H. and A.K. contributed equally to this work.

### Notes

The authors declare no competing financial interest.

## ■ ACKNOWLEDGMENTS

This work was supported as part of the Computational Materials Sciences Program funded by the U.S. Department of Energy, Office of Science, Basic Energy Sciences, under Award Number DE-SC00014607. The simulations were performed at the Argonne Leadership Computing Facility under the DOE INCITE program and at the Center for High Performance Computing of the University of Southern California. S.H. thanks Prof. Adri van Duin for providing valuable information on initial ReaxFF force field parameters for Mo/O/S elements.

## ■ REFERENCES

- Gupta, A.; Sakthivel, T.; Seal, S. *Prog. Mater. Sci.* **2015**, *73*, 44–126.
- Venkata Subbaiah, Y.; Saji, K.; Tiwari, A. *Adv. Funct. Mater.* **2016**, *26*, 2046–2069.
- Zhang, Y.; Tan, Y.-W.; Stormer, H. L.; Kim, P. *Nature* **2005**, *438*, 201–204.
- Qin, Z.; Taylor, M.; Hwang, M.; Bertoldi, K.; Buehler, M. J. *Nano Lett.* **2014**, *14*, 6520–6525.
- Shahil, K. M.; Balandin, A. A. *Solid State Commun.* **2012**, *152*, 1331–1340.
- Li, X.; Zhu, H. *J. Materomics* **2015**, *1*, 33–44.
- Mak, K. F.; Lee, C.; Hone, J.; Shan, J.; Heinz, T. F. *Phys. Rev. Lett.* **2010**, *105*, 136805.
- Nair, R. R.; Ren, W.; Jalil, R.; Riaz, I.; Kravets, V. G.; Britnell, L.; Blake, P.; Schedin, F.; Mayorov, A. S.; Yuan, S. *Small* **2010**, *6*, 2773–2773.
- Kaplan, D.; Gong, Y.; Mills, K.; Swaminathan, V.; Ajayan, P.; Shirodkar, S.; Kaxiras, E. *2D Mater.* **2016**, *3*, 015005.
- Wang, Q. H.; Kalantar-Zadeh, K.; Kis, A.; Coleman, J. N.; Strano, M. S. *Nat. Nanotechnol.* **2012**, *7*, 699–712.
- Lee, G.-H.; Yu, Y.-J.; Cui, X.; Petrone, N.; Lee, C.-H.; Choi, M. S.; Lee, D.-Y.; Lee, C.; Yoo, W. J.; Watanabe, K. *ACS Nano* **2013**, *7*, 7931–7936.
- Pu, J.; Yomogida, Y.; Liu, K.-K.; Li, L.-J.; Iwasa, Y.; Takenobu, T. *Nano Lett.* **2012**, *12*, 4013–4017.
- Li, H.; Tsai, C.; Koh, A. L.; Cai, L.; Contryman, A. W.; Fragapane, A. H.; Zhao, J.; Han, H. S.; Manoharan, H. C.; Abild-Pedersen, F.; Nørskov, J. K.; Zheng, X. *Nat. Mater.* **2015**, *15*, 48.
- Zhang, W.; Zhang, P.; Su, Z.; Wei, G. *Nanoscale* **2015**, *7*, 18364–18378.
- Lv, Z.; Mahmood, N.; Tahir, M.; Pan, L.; Zhang, X.; Zou, J.-J. *Nanoscale* **2016**, *8*, 18250–18269.
- Yu, J.; Li, J.; Zhang, W.; Chang, H. *Chem. Sci.* **2015**, *6*, 6705–6716.
- Ganatra, R.; Zhang, Q. *ACS Nano* **2014**, *8*, 4074–4099.
- Lee, Y. H.; Zhang, X. Q.; Zhang, W.; Chang, M. T.; Lin, C. T.; Chang, K. D.; Yu, Y. C.; Wang, J. T. W.; Chang, C. S.; Li, L. J. *Adv. Mater.* **2012**, *24*, 2320–2325.
- van der Zande, A. M.; Huang, P. Y.; Chenet, D. A.; Berkelbach, T. C.; You, Y.; Lee, G.-H.; Heinz, T. F.; Reichman, D. R.; Muller, D. A.; Hone, J. C. *Nat. Mater.* **2013**, *12*, 554–561.
- Liu, Z.; Amani, M.; Najmaei, S.; Xu, Q.; Zou, X.; Zhou, W.; Yu, T.; Qiu, C.; Birdwell, A. G.; Crowne, F. J. *Nat. Commun.* **2014**, *5*, 5246.
- Lin, Y.-C.; Zhang, W.; Huang, J.-K.; Liu, K.-K.; Lee, Y.-H.; Liang, C.-T.; Chu, C.-W.; Li, L.-J. *Nanoscale* **2012**, *4*, 6637–6641.
- Jeon, J.; Lee, J.; Yoo, G.; Park, J.-H.; Yeom, G. Y.; Jang, Y. H.; Lee, S. *Nanoscale* **2016**, *8*, 16995–17003.
- Zhan, Y.; Liu, Z.; Najmaei, S.; Ajayan, P. M.; Lou, J. *Small* **2012**, *8*, 966–971.
- Mo, Y.; Turner, K. T.; Szlufarska, I. *Nature* **2009**, *457*, 1116–1119.
- Mueller, J. E.; van Duin, A. C. T.; Goddard, W. A., III *J. Phys. Chem. C* **2010**, *114*, 4939–4949.
- Liang, T.; Devine, B.; Phillipot, S. R.; Sinnott, S. B. *J. Phys. Chem. A* **2012**, *116*, 7976–7991.
- Shan, T.-R.; Devine, B. D.; Hawkins, J. M.; Asthagiri, A.; Phillipot, S. R.; Sinnott, S. B. *Phys. Rev. B: Condens. Matter Mater. Phys.* **2010**, *82*, 235302.
- van Duin, A. C. T.; Dasgupta, S.; Lorant, F.; Goddard, W. A. *J. Phys. Chem. A* **2001**, *105*, 9396–9409.
- Liang, T.; Shin, Y. K.; Cheng, Y.-T.; Yilmaz, D. E.; Vishnu, K. G.; Verners, O.; Zou, C.; Phillipot, S. R.; Sinnott, S. B.; van Duin, A. C. T. *Annu. Rev. Mater. Res.* **2013**, *43*, 109–129.
- Chenoweth, K.; van Duin, A. C. T.; Goddard, W. A. *Angew. Chem., Int. Ed.* **2009**, *48*, 7630–7634.
- Ostadhosseini, A.; Rahnamoun, A.; Wang, Y.; Zhao, P.; Zhang, S.; Crespi, V. H.; van Duin, A. C. T. *J. Phys. Chem. Lett.* **2017**, *8*, 631–640.
- Castro-Marcano, F.; Kamat, A. M.; Russo, M. F.; van Duin, A. C. T.; Mathews, J. P. *Combust. Flame* **2012**, *159*, 1272–1285.
- Sentle, T. P.; Hong, S.; Islam, M. M.; Kylasa, S. B.; Zheng, Y.; Shin, Y. K.; Junkermeier, C.; Engel-Herbert, R.; Janik, M. J.; Aktulgah, H. M.; Verstraelen, T.; Grama, A.; van Duin, A. C. T. *npj Comput. Mater.* **2016**, *2*, 15011.
- Akimov, A. V.; Prezhdo, O. V. *Chem. Rev.* **2015**, *115*, 5797–5890.
- Nosé, S. *J. Chem. Phys.* **1984**, *81*, 511–519.
- Hoover, W. G. *Phys. Rev. A: At., Mol., Opt. Phys.* **1985**, *31*, 1695.
- Taheri, P.; Wang, J.; Xing, H.; Destino, J. F.; Arik, M. M.; Zhao, C.; Kang, K.; Blizzard, B.; Zhang, L.; Zhao, P. *Mater. Res. Express* **2016**, *3*, 075009.
- Chen, C.; Feng, Z.; Feng, Y.; Yue, Y.; Qin, C.; Zhang, D.; Feng, W. *ACS Appl. Mater. Interfaces* **2016**, *8*, 19004–19011.
- Chen, J.; Tang, W.; Tian, B.; Liu, B.; Zhao, X.; Liu, Y.; Ren, T.; Liu, W.; Geng, D.; Jeong, H. Y. *Adv. Sci.* **2016**, *3*, 1500033.
- Liu, K.-K.; Zhang, W.; Lee, Y.-H.; Lin, Y.-C.; Chang, M.-T.; Su, C.-Y.; Chang, C.-S.; Li, H.; Shi, Y.; Zhang, H. *Nano Lett.* **2012**, *12*, 1538–1544.
- Liu, H.; Antwi, K. A.; Ying, J.; Chua, S.; Chi, D. *Nanotechnology* **2014**, *25*, 405702.
- Saburi, T.; Murata, H.; Suzuki, T.; Fujii, Y.; Kiuchi, K. *Purazuma&middot;Kaku Yugo Gakkaishi* **2002**, *78*, 3–4.

- (43) Weber, T.; Muijsers, J.; Van Wolput, J.; Verhagen, C.; Niemantsverdriet, J. *J. Phys. Chem.* **1996**, *100*, 14144–14150.  
(44) Li, X. L.; Li, Y. D. *Chem. - Eur. J.* **2003**, *9*, 2726–2731.